Progress In Electromagnetics Research B, Vol. 67, 121–136, 2016

Bistatic Scattering Characteristics of Wheat and Soybean by Radiative Transfer Model in L Band and C Band

Yuan-Yuan Zhang* and Zhen-Sen Wu

Abstract—Compared with the backscattering configuration, the bistatic scattering echoes can provide multidimensional information on land surface. Based on the Michigan Microwave Canopy Scattering (MIMICS) model, a first-order microwave bistatic scattering model for vegetations is developed in this paper. The dominant scattering mechanism for wheat and soybean in the L and C bands is analyzed by simulating the bistatic scattering echoes in multiple viewpoints, which can help us understand the interaction between incident wave and vegetation parameters. The influence of crop height, leaf size and moisture of vegetations and down layer soil on the scattering echoes is fully investigated. The simulations show that the bistatic scattering echoes are more sensitive to the vegetation parameters than that in backscattering configuration. There exist optimal scattering angles, in specular direction and in direction perpendicular to the incident plane, to improve the retrieval accuracy of vegetation parameters and moisture of soil surface. Moreover, the simulations demonstrate that bistatic scattering echoes in high frequency (C band) are a good choice to retrieve the vegetation parameters, and the echoes in low frequency (L band) are preferred to retrieve the soil parameters. This research can be used to provide reference for crop monitoring and future bistatic system design.

1. INTRODUCTION

Wheat and soybean productivity is closely related to the global food security. Meanwhile, electromagnetic scattering and propagation in vegetations play important roles in certain fields such as agricultural production [1], environment change prediction [2], wireless communications [3] and target detection [4]. Recently, research on bistatic scattering [5–10] has received considerable attention because of the multidimensional information provided by bistatic radar systems, which is more than that provided by the monostatic configuration for it only contains 1D data in the backscattering direction. Additional information contained in the bistatic radar has the potential to provide improvements in monitoring vegetation growth and detecting drought degree of crops. Also, the bistatic observations may provide a large scattering echo for targets when the scattering coefficients of the land surface are minimum. This special characteristic can significantly improve the anti-stealth ability of targets for radar system. Therefore, research on bistatic scattering from vegetations is important in providing reference for crop monitoring and target detection, and evidence for a future bistatic radar system design.

Vector radiative transfer (VRT) theory is extensively used in vegetation scattering simulation, where every scattering component has a clear physical meaning. Ulaby et al. [11] first developed the Michigan microwave canopy scattering (MIMICS) model based on the VRT theory and discussed the backscattering characteristics of forests. Toure et al. [12] adapted the MIMICS model to wheat in L and C bands by removing the trunk layer in MIMICS and modifying the scatter distribution density. Mattia et al. [13] investigated the relationship between the backscattering coefficients and wheat biomass, soil

Received 15 January 2016, Accepted 23 March 2016, Scheduled 9 May 2016
* Corresponding author: Yuan-Yuan Zhang (zyy07063@163.com).
The authors are with the School of Physics and Optoelectronic Engineering, Xidian University, Xi'an 710071, China.

moisture in C band. They also addressed the retrieval of the wheat parameters. Huang et al. [14] modified the wheat scattering model in the filling age by adding the ears and verified that the new simulations are in good agreement with the measured backscattering data. Kweon et al. [15] measured the backscattering coefficients of soybean in X band and demonstrated that the simulations based on the first-order VRT model were consistent with the measured backscattering data. Du et al. [16] proposed a new backscattering model for soybean, which included vegetation coherent effect and soil surface curvature. In addition, empirical models are another good choice to predict the scattering echoes of vegetations. Champion et al. [17] developed two semi-empirical models to calculate the backscattering coefficients of wheat. De Roo et al. [18] proposed a semi-empirical backscattering model for soybeans in L and C bands. Kweon and Oh [19] modified the water-cloud empirical model by adding the average and standard deviation of leaf angle distribution to predict the backscattering coefficients of vegetations. Meanwhile, for experiments, Kim et al. [20] conducted backscattering experiments on soybean scattering in L, C, and X bands, and retrieved the leaf area index and vegetation water content by backscattering coefficients in temporal changes. Jia et al. [21] measured the backscattering coefficients of wheat and rice fields in L, S, C and X bands for incident angles of $0^\circ \sim 80^\circ$, and they further investigated the radar sensitivity to canopy variables.

However, the existing models and the experimental research on vegetations have exclusively concentrated on the backscattering direction. The bistatic scattering characteristics of land surface have recently become a subject of increasing interest; however, the main focus of attention is on the rough surface [5, 6, 22–24]. The bistatic scattering from vegetations in the same plane configuration and out-of-plane situations is extremely scarce. Accordingly, there only a few forest scattering works have been reported. In 2002, McLaughlin et al. [25] discussed the full polarization bistatic scattering from forest hills at grazing incident for $28^\circ \sim 66^\circ$ azimuth scattering angles. In 2005, Liang et al. [26] extended the forest backscattering MIMICS to bistatic scattering configuration and reported that an accurate retrieval of results for forest biomass and tree height may be obtained using bistatic scattering radar echoes. In 2000, Ferrazzoli et al. [27] found that the bistatic scattering configuration can overcome the saturation problems occurring in vegetation biomass retrieval at the backscattering direction in L and C bands. In 2015, Gupta et al. [8] measured the rice bistatic scattering coefficients in temporal changes at X band and retrieved crop growth variables using two types of neural network models. When it comes to the work of bistatic scattering interactions between incident waves and wheat and soybean parameters, few research works have been conducted.

Therefore, this study investigates the bistatic scattering characteristics of wheat and soybean using first-order radiative transfer theory. Rest of the paper is organized as follows. Section 2 presents the development of the bistatic scattering model for vegetations. Section 3 validates the bistatic scattering model by the measured backscattering data and discusses the dominant scattering mechanism for wheat and soybean in the L and C bands. The sensitivity of bistatic scattering echoes on crop height, leaf size, and moisture of crops and soil is also investigated. Section 4 concludes the study.

2. BISTATIC SCATTERING MODEL FOR AGRICULTURE

Agriculture is considered as a random medium, which constitutes leaves, stems and branches (Figure 1). Soil under vegetations is usually assumed to be a rough surface. The leaves are regarded as elliptical disks with diameter and thickness. The stems and branches are modeled as needled scatters and finite cylinders, respectively. In this paper, the generalized Rayleigh-Gans (GRG) approximation [28] is used to calculate the scattering amplitude of disk-shaped and needle-shaped scatters, which is valid for a scatter whose least physical dimension d satisfies $k_0 d(\varepsilon_r - 1) \ll 1$. Besides, an approximation derived from the infinite cylinder is used to calculate the scattering field of the finite cylinders for branches. In addition, the permittivity of various canopy constituents can be determined from moisture and frequency through empirical models [29].

As shown in Figure 1, vector $\vec{k}$ refers to the incident or scattering wave, and $\overrightarrow{v}$ and $\vec{h}$ refer to vectors in the vertical and horizontal directions with respect to the horizontal plane, respectively. The crop height is denoted as d. The incident intensity $\vec{I}(\pi - \theta_i, \phi_i, z)$ impinges on the top surface of the canopy, whereas the scattering intensity is expressed as $\vec{I}(\theta_s, \phi_s, z)$ in the free space (Figure 1). The bistatic scattering coefficients of vegetations σ^0_{pq}, which correspond to the q-polarized incident plane

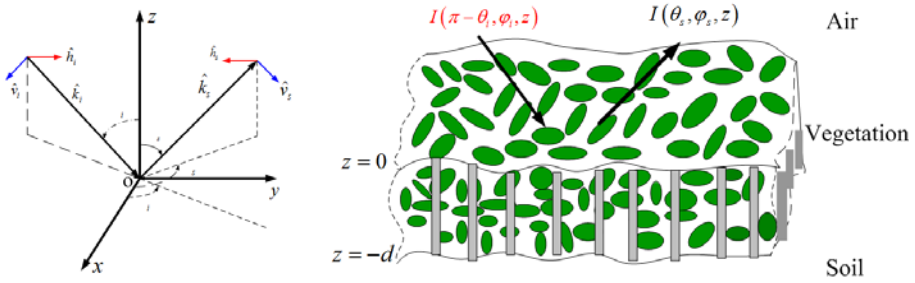

Figure 1. Two-layer scattering model for agriculture.

wave and p-polarized scattering spherical wave, are defined as follows [11]:

$$\sigma_{pq}\left(\theta_s,\phi_s;\pi-\theta_i,\phi_i\right)=\frac{4\pi\cos\theta I_p\left(\theta_s,\phi_s,0\right)}{I_q\left(\pi-\theta_i,\phi_i,0\right)} \tag{1}$$

Then, VRT theory is used to find solution $I(\theta_s,\phi_s,z)$ for the bistatic scattering echoes from vegetations. It describes the scattering, attenuation and absorption in the layers, and can be expressed as:

$$\frac{d\vec{I}(\vec{r},\hat{s})}{ds}=-\bar{\bar{K}}_c\cdot\vec{I}(\vec{r},\hat{s})+\int\limits_{4\pi}d\Omega'\bar{\bar{P}}(\vec{r},\hat{s},\hat{s}')\vec{I}(\vec{r},\hat{s}') \tag{2}$$

where $\vec{I}(\vec{r},\hat{s})$ is the intensity in the vegetation layers and $\bar{\bar{K}}_c$ the extinction matrix that describes the attenuation and absorption caused by the scatters. The phase matrix $\bar{\bar{P}}(\vec{r},\hat{s},\hat{s}')$ represents the scattering energy transfer from direction $\hat{s}'$ to direction $\hat{s}$.

Based on the forward scattering theorem, $\bar{\bar{K}}_c$ can be described as:

$$\begin{aligned}\bar{\bar{k}}_c(\hat{k}_s,\hat{k}_i)&=\frac{4\pi}{k}n_0\mathrm{Im}\left\langle f_{pq}\left(\theta_s,\phi_s,\theta_i,\phi_i\right)\right\rangle\\&=\frac{2\pi}{k}n_0\begin{bmatrix}2\mathrm{Im}\left\langle f_{vv}\right\rangle & 0 & \mathrm{Im}\left\langle f_{vh}\right\rangle & -\mathrm{Re}\left\langle f_{vh}\right\rangle\\ 0 & 2\mathrm{Im}\left\langle f_{hh}\right\rangle & \mathrm{Im}\left\langle f_{hv}\right\rangle & \mathrm{Re}\left\langle f_{hv}\right\rangle\\ 2\mathrm{Im}\left\langle f_{hv}\right\rangle & 2\mathrm{Im}\left\langle f_{vh}f_{hh}^*\right\rangle & \mathrm{Im}\left\langle f_{vv}+f_{hh}\right\rangle & \mathrm{Re}\left\langle f_{vv}-f_{hh}\right\rangle\\ 2\mathrm{Re}\left\langle f_{hv}\right\rangle & -2\mathrm{Re}\left\langle f_{vh}\right\rangle & \mathrm{Re}\left\langle f_{hh}-f_{vv}\right\rangle & \mathrm{Im}\left\langle f_{vv}+f_{hh}\right\rangle\end{bmatrix}\end{aligned} \tag{3}$$

where n_0 is the number of scatters in a unit volume and f_{pq} the scattering amplitude of a scatter in vegetations. If the scatters are isotropic, then $\bar{\bar{K}}_c$ can be reduced to the diagonal form. Furthermore, if the particles are also spherical scatters, $\bar{\bar{K}}_c$ can be expressed as a constant.

The phase matrix $\bar{\bar{P}}$ represents the scattering effect from the incident angle (θ_i,ϕ_i) to the scattering angle (θ_s,ϕ_s), which can be expressed as:

$$\begin{aligned}\bar{\bar{P}}(\theta_s,\phi_s,\theta_i,\phi_i)&=\sum_{m=1}^{N}n_m\left\langle\bar{\bar{P}}_m\right\rangle\\&=n_0\begin{bmatrix}|f_{vv}|^2 & |f_{vh}|^2 & \mathrm{Re}(f_{vv}f_{vh}^*) & -\mathrm{Im}(f_{vv}f_{vh}^*)\\ |f_{hv}|^2 & |f_{hh}|^2 & \mathrm{Re}(f_{hv}f_{hh}^*) & -\mathrm{Im}(f_{hv}f_{hh}^*)\\ 2\mathrm{Re}(f_{vv}f_{hv}^*) & 2\mathrm{Re}(f_{vh}f_{hh}^*) & \mathrm{Re}(f_{vv}f_{hh}^*+f_{vh}f_{hv}^*) & -\mathrm{Im}(f_{vv}f_{hh}^*-f_{vh}f_{hv}^*)\\ 2\mathrm{Im}(f_{vv}f_{hv}^*) & 2\mathrm{Im}(f_{vh}f_{hh}^*) & \mathrm{Im}(f_{vv}f_{hh}^*+f_{vh}f_{hv}^*) & \mathrm{Re}(f_{vv}f_{hh}^*-f_{vh}f_{hv}^*)\end{bmatrix}\end{aligned} \tag{4}$$

The intensity vector in the vegetation layers can be divided into the upward-going $(\vec{I}(\theta,\phi,z))$ and downward-going $(\vec{I}(\pi-\theta,\phi,z))$ components. Thus, the radiative transfer equations in Eq. (2) are expressed as:

$$\begin{cases}\cos\left(\theta\right)\dfrac{d\vec{I}(\theta,\phi,z)}{dz}=-\bar{\bar{K}}_c(\theta)\cdot\vec{I}(\theta,\phi,z)+\vec{S}_c(\theta,\phi,z), & -d\le z\le 0\\ -\cos\left(\theta\right)\dfrac{d\vec{I}(\pi-\theta,\phi,z)}{dz}=-\bar{\bar{K}}_c(\pi-\theta)\cdot\vec{I}(\pi-\theta,\phi,z)+\vec{S}_c(\pi-\theta,\phi,z), & -d\le z\le 0\end{cases} \tag{5}$$

As shown in Eq. (5), $\bar{\bar{K}}_c(\pi-\theta)$ and $\bar{\bar{K}}_c(\theta)$ are the extinction matrices in the downward-going and upward-going directions for the vegetation layers, respectively. And also, $\vec{S}_c(\pi-\theta,\phi,z)$ and $\vec{S}_c(\theta,\phi,z)$ are the scattering source functions in the downward-going and upward-going directions, respectively.

The effective canopy layer permittivity is small for the small volume fraction of leaves and large volume fraction of air. Thus, the refection at the boundary layer between air and canopy layers is ignored, and only transmission between the layers is considered. Meanwhile, the incident intensity is reflected at the relatively flat soil surface through vegetations. Therefore, the boundary conditions are described as:

$$\vec{I}(\pi-\theta_i,\phi_i,0)=\vec{I}_0^i \tag{6}$$

$$\vec{I}(\theta_s,\phi_s,-d)=\int_0^{\pi/2}d\theta'\sin\theta'\int_0^{2\pi}d\varphi'\vec{I}(\pi-\theta',\phi',-d)\,\bar{\bar{G}}(\theta_s,\phi_s;\pi-\theta',\phi') \tag{7}$$

where $\bar{\bar{G}}$ is the phase matrix of the rough soil surface, and the soil scattering coefficients are derived as $\sigma_g=4\pi\cos\theta_s\bar{\bar{G}}$.

If the extinction rate of scatters is small, then the solution of Eq. (5) can be expressed in the form of perturbation series. After solving the equations iteratively, the bistatic scattering coefficients of vegetations can be expressed as:

$$\begin{aligned}&\vec{I}(\theta_s,\phi_s;\pi\text{ - }\theta_i,\phi_i,z)\\&=\exp\left[-\bar{\bar{K}}_c(\theta_s)(z+d)\sec\theta_s\right]\cdot\int_0^{\pi/2}d\theta'\sin\theta'\int_0^{2\pi}d\varphi'\vec{I}(\pi-\theta_i,\phi_i,-d)\,\bar{\bar{G}}(\theta,\phi;\pi-\theta_i,\phi_i)\\&+\sum_{n=1}^{\infty}\int_{-d}^{z}dz'\exp\left[-\bar{\bar{K}}_c(\theta_s)(z-z')\sec\theta_s\right]\vec{\vec{S}}_c^{\,n}(\theta_s,\phi_s;\theta_i,\phi_i,z')\sec\theta_s\end{aligned} \tag{8}$$

Where

$$\vec{\vec{S}}_c^{\,n}(\theta,\phi,z)=\int_0^{2\pi}d\phi'\int_0^{\frac{\pi}{2}}\sin\theta'd\theta'\left[\bar{\bar{P}}_c(\theta,\phi,\theta',\phi')\cdot\vec{\vec{I}}_c^{\,n-1}(\theta',\phi',z)+\bar{\bar{P}}_c(\theta,\phi,\pi-\theta',\phi')\cdot\vec{\vec{I}}_c^{\,n-1}(\pi-\theta',\phi',z)\right] \tag{9}$$

$$\begin{aligned}\vec{\vec{S}}_c^{\,n}(\pi-\theta,\phi,z)\;=\;&\int_0^{2\pi}d\phi'\int_0^{\frac{\pi}{2}}\sin\theta'd\theta'\left[\bar{\bar{P}}_c(\pi-\theta,\phi,\theta',\phi')\cdot\vec{\vec{I}}_c^{\,n-1}(\theta',\phi',z)\right.\\&\left.+\bar{\bar{P}}_c(\pi-\theta,\phi,\pi-\theta',\phi')\cdot\vec{\vec{I}}_c^{\,n-1}(\pi-\theta',\phi',z)\right]\end{aligned} \tag{10}$$

(1) Zero-order Solutions

As shown in Eqs. (9) and (10), if the phase matrix is assumed to be zero, then source function is zero, and the incident wave is only reflected by soil surface. Therefore, the zero-order solution of the VRT model corresponds to land scattering, and can be described as

$$\vec{\vec{I}}^{\,0}(\theta_s,\phi_s;\pi-\theta_i,\phi_i,z)=\exp\left[-\bar{\bar{K}}_c(\theta_s)(z+d)\sec\theta_s\right]\exp\left[-\bar{\bar{K}}_c(\pi-\theta_i)d\sec\theta_i\right]\bar{\bar{G}}(\theta_s,\phi_s;\pi-\theta_i,\phi_i) \tag{11}$$

where $\exp[-\bar{\bar{K}}_c(\pi-\theta_i)d\sec\theta_i]$ and $\exp[-\bar{\bar{K}}_c(\theta_s)(z+d)\sec\theta_s]$ are the attenuations in the incident and scattering directions, respectively. When $z=0$, the bistatic scattering coefficients of the land surface can be expressed as:

$$\sigma_{pq}^0(\theta_s,\phi_s;\pi-\theta_i,\phi_i,0)=\exp\left[-\bar{\bar{K}}_c(\theta_s)d\sec\theta_s\right]\sigma_{pq}^g(\theta_s,\phi_s;\pi-\theta_i,\phi_i)\exp\left[-\bar{\bar{K}}_c(\pi-\theta_i)d\sec\theta_i\right] \tag{12}$$

(2) First-order Solutions

Assuming that $n=1$ in Eq. (9), then first-order intensity for the upward-going $\vec{\vec{I}}^{\,1}(\theta,\phi,z)$ and downward-going $\vec{\vec{I}}_c^{\,1}(\pi-\theta,\phi,z)$ components can be described as:

$$\vec{\vec{I}}^{\,1}(\pi-\theta,\phi,z)=\int_z^0dz'\exp\left[\bar{\bar{K}}_c(\pi-\theta)(z-z')\sec\theta\right]\vec{\vec{S}}_c^{\,1}(\pi-\theta,\phi,z')\sec\theta \tag{13}$$

$$\begin{aligned}\vec{\vec{I}}^{1}(\theta,\phi,z) \;=\; &= \exp\left[-\bar{\bar{K}}_c(\theta)(z+d)\sec\theta\right]\cdot\int_0^{\pi/2}d\theta'\sin\theta'\int_0^{2\pi}d\phi'\bar{\bar{G}}\left(\theta,\phi;\pi-\theta',\phi'\right)\\ &\cdot\left[\int_{-d}^{0}dz'\exp\left[\bar{\bar{K}}_c(\pi-\theta')(-d-z')\sec\theta'\right]\vec{\vec{S}}_c^{1}(\pi-\theta',\phi',z')\sec\theta'\right]\\ &+\sum_{n=1}^{\infty}\int_{-d}^{z}dz'\exp\left[-\bar{\bar{K}}_e(\theta)(z-z')\sec\theta\right]\vec{\vec{S}}_c^{1}(\theta,\phi,z')\sec\theta \qquad (14)\end{aligned}$$

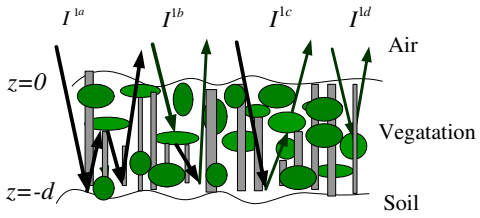

Figure 2. Bistatic scattering terms for first-order solutions.

Then, the first-order upward-going scattering intensity $\vec{I}^{1}(\theta_s,\phi_s;\theta_i,\phi_i,z)$ for the vegetations can be expressed as the sum of four components, namely, $\vec{I}^{1a}(\theta_s,\phi_s;\pi-\theta_i,\phi_i,z)$, $\vec{I}^{1b}(\theta_s,\phi_s;\pi-\theta_i,\phi_i,z)$, $\vec{I}^{1c}(\theta_s,\phi_s;\pi-\theta_i,\phi_i,z)$ and $\vec{I}^{1d}(\theta_s,\phi_s;\pi-\theta_i,\phi_i,z)$ (Figure 2). The term $\vec{I}^{1a}(\theta_s,\phi_s;\pi-\theta_i,\phi_i,z)$ for ground-vegetation-ground scattering is expressed as

$$\begin{aligned}&\vec{I}^{1a}(\theta_s,\phi_s;\pi-\theta_i,\phi_i,z)\\ &=\exp\left[-\bar{\bar{K}}_c(\theta_s)(z+d)\sec\theta_s\right]\cdot\exp\left[-\bar{\bar{K}}_c(\pi-\theta_i)d\sec\theta_i\right]\overline{I}_0^{i}\int_0^{\pi/2}d\theta'\sin\theta'\int_0^{2\pi}d\phi'\bar{\bar{G}}\left(\theta,\phi;\pi-\theta',\phi'\right)\sec\theta'\\ &\cdot\exp\left[-\bar{\bar{K}}_c(\pi-\theta')d\sec\theta'\right]\cdot\int_0^{2\pi}d\phi''\int_0^{\frac{\pi}{2}}\sin\theta''d\theta''\left[\bar{\bar{P}}_c(\pi-\theta',\phi',\theta'',\phi'')\cdot\right.\\ &\left.\cdot\left[\exp[-\bar{\bar{K}}_c(\theta'')d\sec\theta'']\bar{\bar{G}}\left(\theta'',\phi'';\pi-\theta_i,\phi_i\right)\right]\cdot\frac{\left\{\exp[\bar{\bar{K}}_c(\pi-\theta')d\sec\theta'+\bar{\bar{K}}_c(\theta'')d\sec\theta'']-1\right\}}{\bar{\bar{K}}_c(\pi-\theta')\sec\theta'+\bar{\bar{K}}_c(\theta'')\sec\theta''} \qquad (15)\end{aligned}$$

The term $I_c^{1b}(\theta_s,\phi_s;\pi$ - $\theta_i,\phi_i,z)$ for vegetation-ground scattering is given as:

$$\begin{aligned}&\vec{I}^{1b}(\theta_s,\phi_s;\pi-\theta_i,\phi_i,z)\\ &=\exp\left[-\bar{\bar{K}}_c(\theta_s)(z+d)\sec\theta_s\right]\cdot\int_0^{\pi/2}d\theta'\sin\theta'\int_0^{2\pi}d\phi'\bar{\bar{G}}\left(\theta_s,\phi_s;\pi-\theta',\phi'\right)\\ &\cdot\bar{\bar{P}}_c(\pi-\theta',\phi',\pi-\theta_i,\phi_i)\cdot\overline{I}_0^{i}\sec\theta'\frac{\left\{\exp\left[-\bar{\bar{K}}_c(\pi-\theta')d\sec\theta'\right]-\exp\left[-\bar{\bar{K}}_c(\pi-\theta_i)d\sec\theta_i\right]\right\}}{\bar{\bar{K}}_c(\pi-\theta_i)\sec\theta_i-\bar{\bar{K}}_c(\pi-\theta')\sec\theta'} \qquad (16)\end{aligned}$$

The term $I_c^{1c}(\theta_s,\phi_s;\pi-\theta_i,\phi_i,z)$ for ground-vegetation scattering is described as

$$\begin{aligned}&\vec{I}^{1c}(\theta_s,\phi_s;\pi-\theta_i,\phi_i,z)\\ &=\exp\left[-\bar{\bar{K}}_e(\theta_s)z\sec\theta_s\right]\cdot\exp\left[-\bar{\bar{K}}_c(\pi-\theta_i)d\sec\theta_i\right]\sec\theta\vec{\vec{I}}_0^{i}\int_0^{2\pi}d\phi'\int_0^{\frac{\pi}{2}}\sin\theta'd\theta'\bar{\bar{P}}_c(\theta_s,\phi_s,\theta',\phi')\\ &\cdot\bar{\bar{G}}\left(\theta',\phi';\pi-\theta_i,\phi_i\right)\cdot\frac{\exp\left[\bar{\bar{K}}_e(\theta_s)z\sec\theta-\bar{\bar{K}}_c(\theta')z\sec\theta'-\bar{\bar{K}}_c(\theta')d\sec\theta'\right]-\exp\left[-\bar{\bar{K}}_e(\theta_s)d\sec\theta_s\right]}{\bar{\bar{K}}_e(\theta_s)\sec\theta_s-\bar{\bar{K}}_c(\theta')\sec\theta'} \qquad (17)\end{aligned}$$

The term $I_c^{1d}(\theta_s, \phi_s; \pi - \theta_i, \phi_i, z)$ for direct vegetation scattering is expressed as

$$\begin{aligned}&\vec{I}^{1d}(\theta_s, \phi_s; \pi - \theta_i, \phi_i, z)\\&= \exp\left[-\bar{\bar{K}}_e(\theta_s) z \sec\theta_s\right] \bar{\bar{P}}_c(\theta_s, \phi_s; \pi - \theta_i, \phi_i) \cdot \sec\theta_s \cdot \overline{I}_0^i\\&\cdot \frac{\exp\left[\bar{\bar{K}}_e(\theta_s) z \sec\theta_s + \bar{\bar{K}}_c(\pi - \theta_i) z \sec\theta_i\right] - \exp\left[-\bar{\bar{K}}_e(\theta_s) d \sec\theta_s - \bar{\bar{K}}_c(\pi - \theta_i) d \sec\theta_i\right]}{\bar{\bar{K}}_e(\theta_s)\sec\theta_s + \bar{\bar{K}}_c(\pi - \theta_i)\sec\theta_i}\end{aligned} \tag{18}$$

Finally, the total bistatic scattering coefficients $\sigma_{pq}(\theta_s, \phi_s; \pi - \theta_i, \phi_i, 0)$ for the vegetations can be expressed as the sum of the zero-order and first-order solutions for the radiative transfer equations, which are expressed as:

$$\sigma_{pq}(\theta_s, \phi_s; \pi - \theta_i, \phi_i, 0) = \sigma_{pq}^0(\theta_s, \phi_s; \pi - \theta_i, \phi_i, 0) + \sigma_{pq}^1(\theta_s, \phi_s; \pi - \theta_i, \phi_i, 0) \tag{19}$$

where $\sigma_{pq}^0\theta_s, \phi_s; \pi - \theta_i, \phi_i, 0)$ is given in Eq. (12), and $\sigma_{pq}^1(\theta_s, \phi_s; \pi - \theta_i, \phi_i, 0)$ is described as follows:

$$\sigma_{pq}^1(\theta_s, \phi_s; \pi - \theta_i, \phi_i, 0) = \frac{4\pi\cos\theta_s}{\overline{I}_0^i} \left\{ \begin{array}{l} \vec{I}^{1a}(\theta_s, \phi_s; \pi - \theta_i, \phi_i, 0) + \vec{I}^{1b}(\theta_s, \phi_s; \pi - \theta_i, \phi_i, 0) \\ +\vec{I}^{1c}(\theta_s, \phi_s; \pi - \theta_i, \phi_i, 0) + \vec{I}^{1d}(\theta_s, \phi_s; \pi - \theta_i, \phi_i, 0) \end{array} \right\} \tag{20}$$

3. RESULTS AND DISCUSSION

3.1. Model Validation by the Measured Backscattering Data

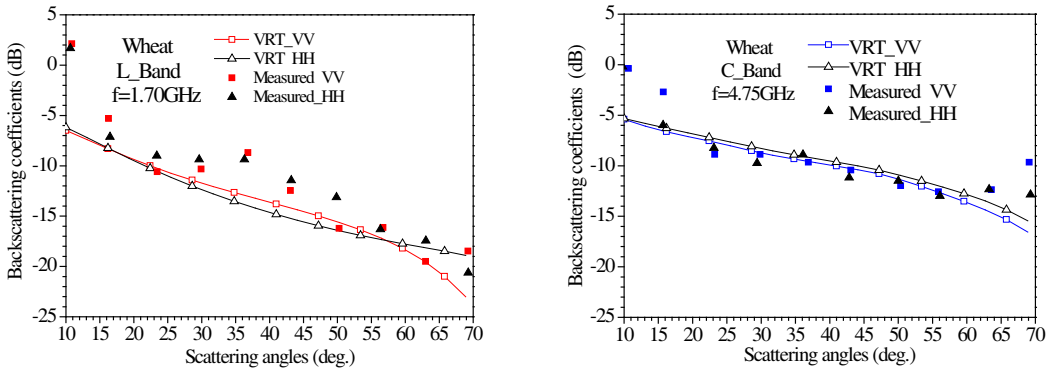

Figure 3. Comparison of simulated and measured data for wheat (a) $f = 1.70$ GHz (b) $f = 4.75$ GHz.

For measured bistatic scattering data of vegetations are scarce, $\theta_s = \theta_i$, $\varphi_i = 0$, $\varphi_s = \pi$ are set to validate the bistatic scattering model developed in this study. Table 1 shows the input parameters of wheat [12]. Then, the wheat backscattering coefficients simulated by the model are compared with the measured data [12] in the L and C bands. As shown in Figure 3, the consistency between the simulated data and the measured backscattering data indicates the correctness of the bistatic scattering model.

Table 1. The input parameters of wheat.

Stem	Leaf	Soil
moisture: 0.72 (g/g)	moisture: 0.67 (g/g)	moisture: 0.17 (g/cm^3)
height: 50 cm	length: 120 mm	RMS: 1.2 cm
radius: 1 mm	width: 10 mm	correlation length: 4.9 cm
density: 320/m^3	thickness: 0.2 mm	vegetation height: 50 cm
PDF: vertical	density: 3430/m^3	PDF: uniform

3.2. Bistatic Scattering Mechanisms of Wheat and Soybean

The crops can be divided into narrow-leafy crops and broad-leafy crops depending on the leaf shape. Analysis on the bistatic scattering characteristics of these two crop types is given in the subsequent sections. Wheat is an example of a narrow-leaved crop, whereas soybean is an example of a broad-leaved crop. Tables 1 and 2 show the physical parameters for wheat [12] and soybean [30], respectively.

Table 2. The input parameters of soybean.

Stem	Leaf	Soil
moisture: 0.6 (g/g)	moisture: 0.6 (g/g)	moisture: 0.3 (g/cm^3)
length: 9 cm	semi-major axis: 4.3 cm	RMS: 1.1 cm
radius: 1.6 mm	semi-minor axis: 4.3 cm	correlation length: 15 cm
density: 124/m^3	thickness: 0.24 mm	vegetation height: 50 cm
PDF: uniform	density: 968/m^3	PDF: uniform

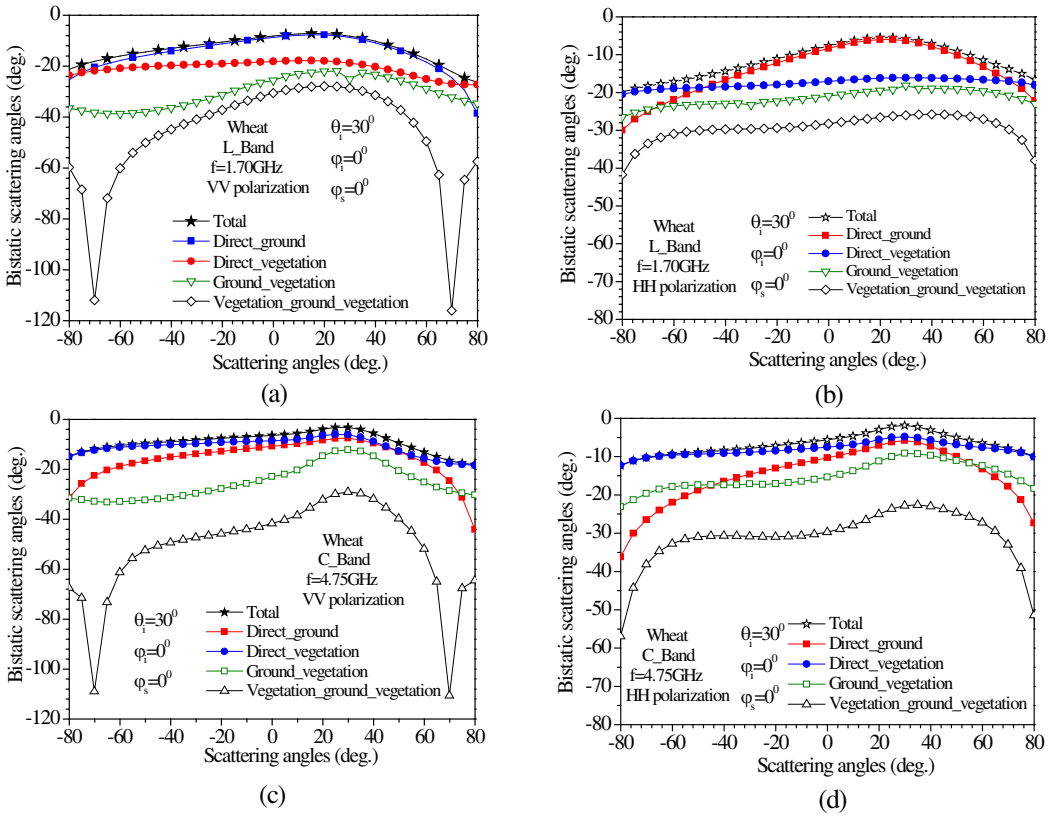

Figure 4. Bistatic scattering components for wheat versus scattering angles. (a) L-VV, (b) L-HH, (c) C-VV, (d) C-HH.

The major part of the bistatic scattering echoes for wheat, at conditions of $\theta_i = 30°$, $\varphi_i = \varphi_s = 0°$, $\theta_s = -80° \sim 80°$ in L band, is the direct soil scattering at small scattering angles, whereas the dominant scattering mechanism for large scattering angles is the direct canopy scattering (Figure 4). When the incident frequency increases, the scattering from the soil surface is significantly reduced for the attenuation caused by vegetations increases, and canopy scattering becomes the strongest effect in the C band. The vegetation-ground scattering component also increases with the increase of frequency. However, the effect of ground-vegetation-ground scattering is low for all cases and can be ignored at L

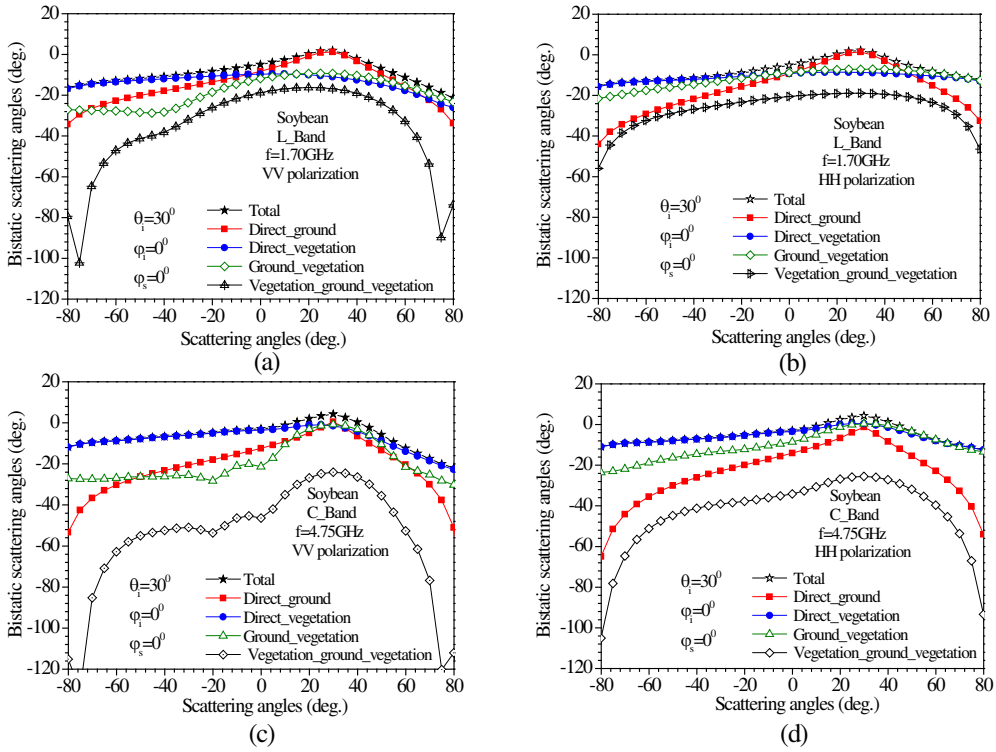

Figure 5. Bistatic scattering components for soybean versus scattering angles. (a) L-VV, (b) L-HH, (c) C-VV, (d) C-HH.

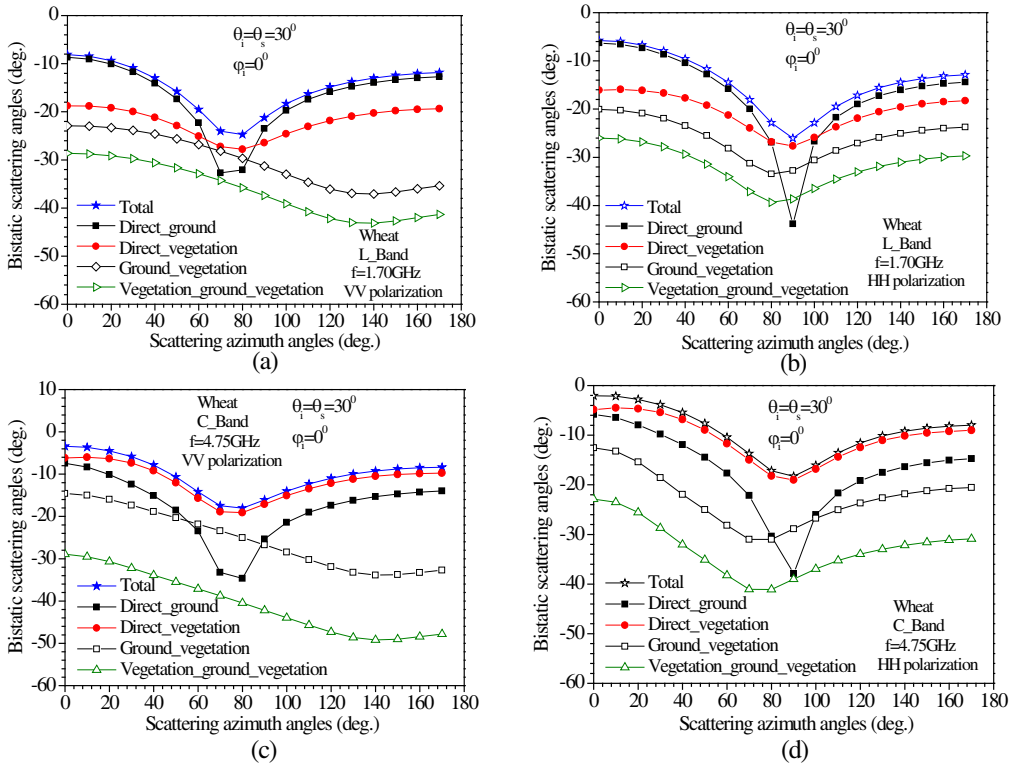

Figure 6. The bistatic scattering components for wheat versus scattering angles. (a) L-VV, (b) L-HH, (c) C-VV, (d) C-HH.

and C bands.

Figure 5 shows the bistatic scattering coefficients of soybean in the L and C bands. Similar to that in backscattering case, bistatic scattering coefficients are also dominated by the soil surface in the L band at low scattering angles and by direct vegetations in the backward scattering plane at high scattering angles. Because the soybean plants are spare, much incident wave can penetrate the vegetation and reach the ground. Consequently, the direct vegetation and the ground-vegetation scattering components are dominant at large scattering angles in the specular scattering plane. In the C band, direct vegetations scattering is the strongest effect in the backscattering plane (Figures 5(c) and 5(d)). However, in the specular scattering plane, the main scattering parts are vegetation and ground-vegetation for HH polarization, and vegetation scattering for VV polarization. The simulated results, shown in Figures 4 and 5, reveal that the bistatic scattering echoes have the potential to retrieve the soil moisture in the specular scattering direction at low frequency and to retrieve the vegetation parameters at large scattering angles in the backscattering plane with high accuracy.

As shown in Figures 6 and 7, when the scattering wave and incident wave are in the different plane, the dominant scattering mechanisms for wheat and soybean are also investigated. The direction $\varphi_s = 0°$ and $\varphi_s = 180°$ refer to the specular and backscattering direction, respectively. The minimum of scattering echoes $\theta_s = \theta_i = 30°$ occurs in the plane perpendicular to the incident plane for HH polarization ($\varphi_s = 90°$). And the minimum tends to be smaller scattering azimuth angles for the VV polarization. Figures 6(a) and 6(b) show that the soil surface for the wheat crops in L band is dominant at the scattering azimuth angles of $0° \leq \varphi_s \leq 60°$ and $90° \leq \varphi_s \leq 180°$. The direct vegetation scattering and the ground-vegetation interaction are the largest scattering components for $60° \leq \varphi_s \leq 90°$. However, the direct vegetation scattering in C band is dominant at the full range of scattering azimuth angles, and the other scattering effects can be ignored (Figures 6(c) and 6(d)).

As shown in Figures 7(a) and 7(b), the soil scattering for soybean in the L band is dominant at small scattering azimuth angles of $0° \leq \varphi_s \leq 40°$, and the vegetations scattering effect is greater than

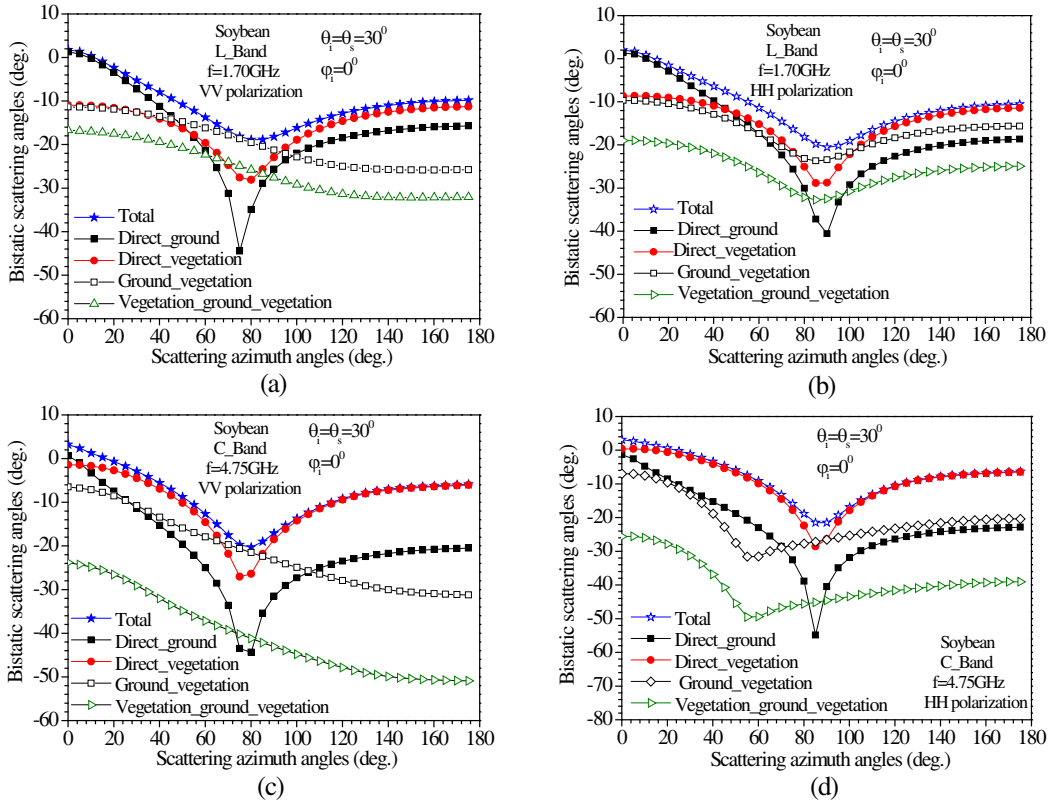

Figure 7. The bistatic scattering components for soybean versus scattering azimuth angles. (a) L-VV, (b) L-HH, (c) C-VV, (d) C-HH.

other scattering components at large scattering azimuth angles of $100^\circ \leq \varphi_s \leq 180^\circ$. In addition, the ground-vegetation scattering component is dominant at the scattering azimuth angles of approximately $40^\circ \leq \varphi_s \leq 90^\circ$ for VV polarization, and at $76^\circ \leq \varphi_s \leq 106^\circ$ for HH polarization. Figures 7(c) and 7(d) show that the direct vegetations scattering component in C band for $\theta_s = \theta_i = 30^\circ$, $\varphi_i = 0^\circ$, $\varphi_s = 0^\circ \sim 180^\circ$ is dominant for almost all scattering azimuth angles. However, the dominant scattering component changes from direct vegetation scattering component to ground-vegetations scattering component in the scattering plane perpendicular to the incident plane. Meanwhile, the soil scattering components give rise to the total scattering echoes by 2 dB in the specular scattering direction. These conclusions can help us understand the bistatic interactions between scattering wave and vegetation parameters and retrieve the vegetation parameters with high accuracy.

3.3. Sensitivity of Scattering Echoes to Vegetation Parameters

The sensitivity of bistatic scattering coefficients to vegetation parameters plays a critical role in the retrieval of canopy parameters and down layer soil moisture. This section discusses the influence of canopy height and leaf size on the soybean scattering coefficients in L and C bands. The sensitivity of the scattering coefficients on vegetation moisture and the soil moisture for the wheat vegetations is also analyzed in L and C bands.

3.3.1. Soybean Parameters Analysis

Figures 8(a) and 8(b) show that the bistatic scattering coefficients of soybean in the specular direction decrease with the increase in the crop height, for the soil surface is dominated in the specular direction

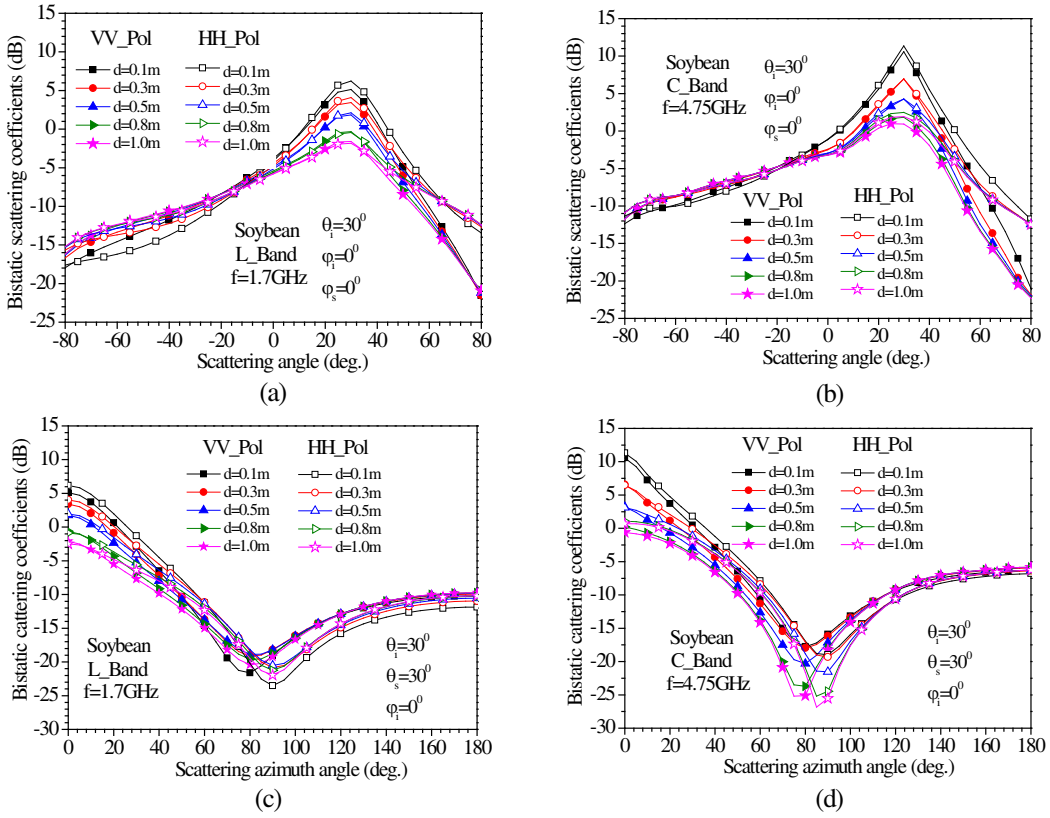

Figure 8. Bistatic scattering coefficients for soybean sensitivity to crop height. (a) L_band bistatic scattering echoes versus scattering angles. (b) C_band bistatic scattering echoes versus scattering angles. (c) L_band bistatic scattering echoes versus scattering azimuth angles. (d) C_band bistatic scattering echoes versus scattering azimuth angles.

and influenced by the large attenuation of vegetations. The largest discrepancies among five different crop heights are observed in the specular direction ($\theta_s = \theta_i = 30°$, $\varphi_i = 0°$, $\varphi_s = 0°$), with values of 6.72 dB and 8.87 dB in L and C bands, respectively. Figures 8(c) and 8(d) show that the total scattering echoes in L and C bands in the specular direction ($\varphi_s = 0°$) decrease obviously with the increase in crop height. The minimum of the scattering coefficients in C band apparently decreases with the increase in soybean height. However, the scattering echoes become saturated with crop height increase in the backscattering configuration ($\varphi_s = 180°$), and no significant difference exists for the five crop heights. Therefore, the bistatic scattering echoes have more potential than the backscattering coefficients in improving the retrieval accuracy of crop height significantly.

Figure 9 shows the scattering coefficients of soybean for three different leaf sizes. DY1 refers to disk-shaped leaves with a diameter of $d_1 = 0.086$ m and a thickness of $h_1 = 0.00024$ m. DY2 refers to the disk-shaped leaves with a diameter of $d_2 = 0.068$ m and a thickness of $h_2 = 0.00018$ m. DY3 refers to disk-shaped leaves with a diameter of $d_3 = 0.068$ m and a thickness of $h_3 = 0.00018$ m. The incident wave is $\theta_i = 30°$, $\varphi_i = 0°$, and the scattering wave is in the incident plane for $\theta_s = -90° \sim 90°$, $\varphi_s = 0°$ (Figures 9(a) and 9(b)). The largest discrepancies between the scattering echoes for three different leaf sizes exist in the specular direction and at large scattering angles in the backscattering plane for L and C bands. With the increase in leave size, the scattering echoes in specular direction decrease for the large attenuation caused by vegetations on the soil surface. However, the scattering echoes increase with the increase in leaf size at large scattering angles in the backscattering plane, where vegetations scattering is dominant.

In Figures 9(c) and 9(d), the scattering wave satisfies $\theta_s = \theta_i = 30°$ and changes with the scattering azimuth angles. The total scattering echoes in the specular direction in L band decrease with the increase

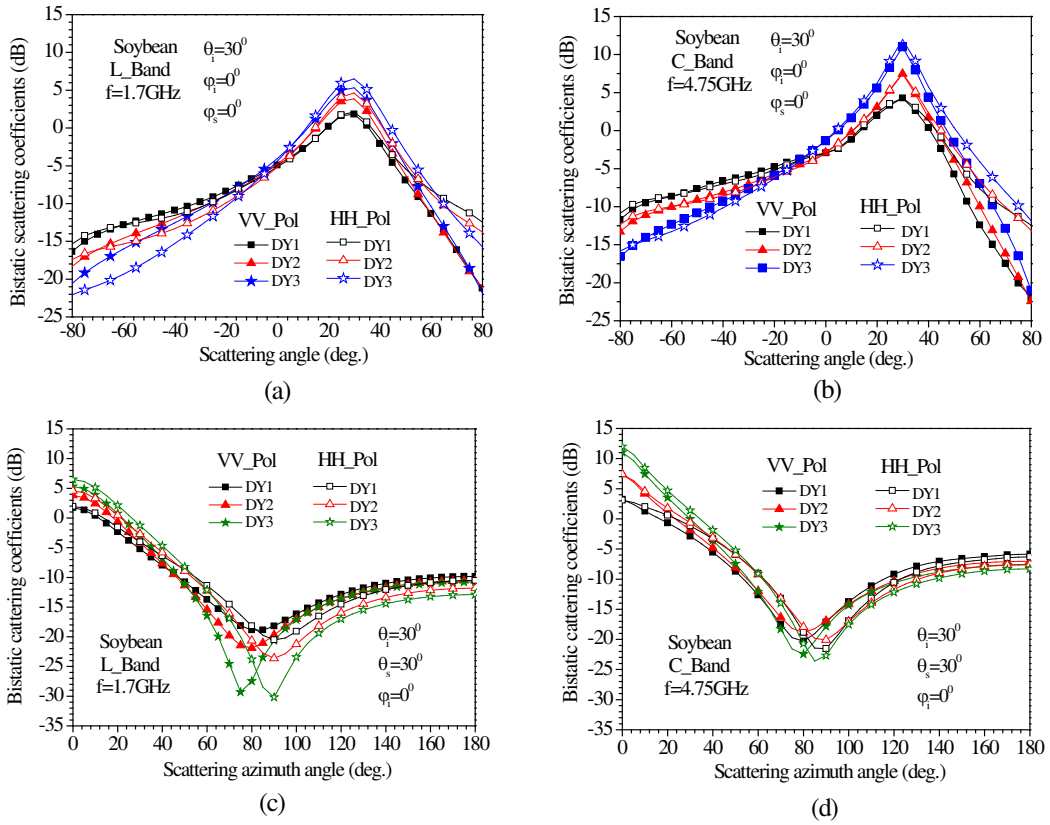

Figure 9. Bistatic scattering coefficients for soybean sensitivity to leaf size. (a) L_band bistatic scattering echoes versus scattering angles. (b) C_band bistatic scattering echoes versus scattering angles. (c) L_band bistatic scattering echoes versus scattering azimuth angles. (d) C_band bistatic scattering echoes versus scattering azimuth angles.

in leave sizes. However, the scattering echoes in backscattering direction increase with the increase in leave size, and the trends are not evident. In C band, the vegetation scattering is dominant for almost all ranges, but the soil scattering cannot be ignored in the specular direction. The leaf size has a significant influence on attenuation compared with that on scattering. Therefore, the total scattering echoes decrease with the increase in leaf size, for the larger attenuation caused by the vegetations on soil surface. The ground-vegetation scattering is the largest scattering component in L and C bands in the direction perpendicular to the incident plane. Thus, the scattering coefficients increase with the increase in leaf size. This effect is particularly significant in L band. These figures show that the scattering echoes in specular direction are a good choice for leaf size retrieval at high frequency, when the backscattering echoes become saturated.

3.3.2. Wheat Parameters Analysis

In this section, a similar sensitivity research is applied to the wheat vegetations. However, the moisture of vegetations and soil surface is investigated instead of changing the crop height and leaf size used for soybean.

As shown in Figure 10(a), the bistatic scattering echoes in L band slightly decrease with the increase in vegetation moisture in the specular direction, for the larger attenuation caused by the vegetations with higher moisture on the soil surface. No significant difference is observed in other scattering angles. In Figure 10(b), the increase in vegetations moisture leads to an increase in the bistatic scattering echoes in C band at large scattering angles in the backscattering plane, where vegetation scattering is dominant. However, a trend of firstly decrease and then increase is observed in the forward scattering

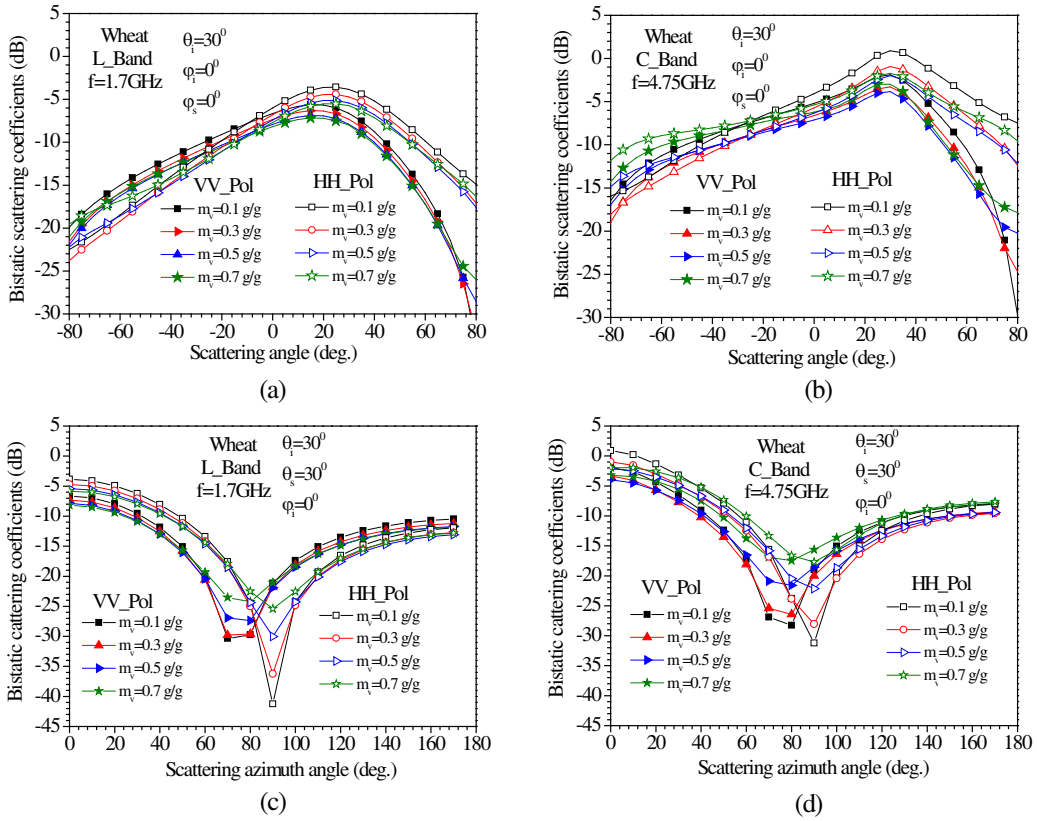

Figure 10. Bistatic scattering coefficients for wheat sensitivity to vegetation moisture. (a) L_band bistatic scattering echoes versus scattering angles. (b) C_band bistatic scattering echoes versus scattering angles. (c) L_band bistatic scattering echoes versus scattering azimuth angles. (d) C_band bistatic scattering echoes versus scattering azimuth angles.

plane, because the dominant scattering effect changes from soil scattering near the specular scattering direction to vegetations at large scattering angles. The scattering echoes in C band are more sensitive to vegetation moisture than those in L band.

Figures 10(c) and 10(d) show that the bistatic scattering echoes of wheat change with the scattering azimuth angles. The two figures show a similar variation trend. The minimum of the scattering angles exists at the scattering plane of $\varphi_s = 90°$ and approximately $\varphi_s = 78°$ for the HH and VV polarizations, respectively. The minimum values increase with the increase in vegetations moisture for vegetation scattering dominant in the direction perpendicular to the incident plane. Meanwhile, the scattering echoes in the specular scattering direction decrease with the increase in vegetations moisture for the large vegetation attenuation on the soil surface, which is dominant here. However, no significant difference among the four vegetations moisture values is observed in the backscattering configuration ($\varphi_s = 180°$).

Figures 11(a) and 11(b) show that the bistatic scattering echoes in the specular direction ($\theta_s = \theta_i = 30°$) for the HH polarization are greater than those for the VV polarization. The scattering coefficients show a significant increase with increase in vegetation moisture when moisture of vegetation is low. However, the speed slows down and gradually saturates when moisture of vegetation is high. The variation range of specular scattering echoes in L band for soil moisture from 0.1 g/cm^3 to 0.8 g/cm^3 is 6.51 dB and 4.29 dB for VV and HH polarizations, respectively. However, in C band, the variation range is 1.15 dB and 1.90 dB for VV and HH polarizations, respectively. Moisture sensitivity in the specular direction for L band is greater than that for C band. Therefore, L band simulations in VV polarization are a good choice in retrieving soil moisture with high accuracy.

The sensitivity of backscattering coefficients for wheat on the soil moisture is also investigated

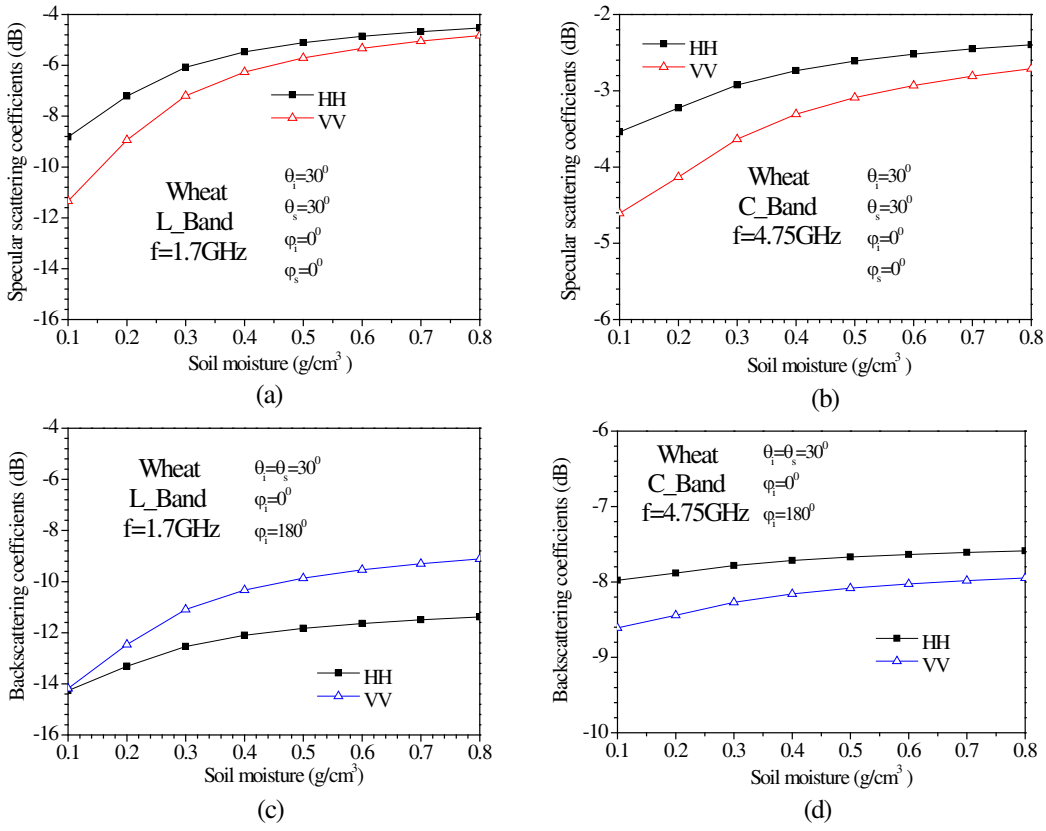

Figure 11. Scattering coefficients for wheat sensitivity to down layer soil moisture. (a) L_band specular scattering echoes versus scattering angles. (b) C_band specular scattering echoes versus scattering angles. (c) L_band backscattering echoes versus scattering angles. (d) C_band backscattering echoes versus scattering angles.

(Figures 11(c) and 11(d)). The backscattering coefficients in VV polarization are greater than those in HH polarization for L band. However, the opposite trend is observed in C band. The variation range of the scattering coefficients for soil moisture from 0.1 g/cm^3 to 0.8 g/cm^3 in L band is 5.08 dB and 2.88 dB for VV and HH polarizations, respectively. Meanwhile, the variation range in C band is 0.66 dB and 0.39 dB for VV and HH polarizations, respectively. The influence of soil moisture becomes evident when soil surface scattering is dominant in the total scattering echoes. A comparison of the variation range of the scattering coefficients with different soil moistures shows that the specular scattering coefficients in low frequency (L band) are more sensitive to soil moisture than backscattering configuration ($\theta_s = 30^\circ$), which is similar to the single rough surface [32, 33].

4. CONCLUSION

This study develops a bistatic scattering model for vegetations based on radiative transfer theory which is validated by wheat measured backscattering data. The bistatic scattering characteristics of wheat and soybean, versus the scattering angles and scattering azimuth angles, are investigated in L and C bands. The sensitivity of the scattering echoes to the crop height, leaf size and moisture of crops and soil is also investigated. The conclusions are summarized as follows:

(1) When the scattering wave and incident wave are in the same plane, the dominant bistatic scattering effect for wheat and soybean in L band is the soil scattering for the scattering angles near the specular direction. However, it changes to vegetation scattering when scattering angles are far from the specular direction. In C band, the vegetations scattering is dominant at the full range of the scattering angles, and the soil scattering effect cannot be ignored near the specular direction. When the scattering echoes for $\theta_s = \theta_i$, $\varphi_i = 0^\circ$ change with the scattering azimuth angles in L band, soil surface scattering is dominant for almost all range of scattering angles, except for the scattering angles near the perpendicular plane, where it is dominated by vegetation scattering for wheat and by ground-vegetations scattering for soybean. In C band, the dominant scattering effect for wheat and soybean is vegetation scattering at the full range, except for soybean in the perpendicular plane, where ground-vegetations scattering is dominant.

(2) The dominant scattering mechanisms are related to the sensitivity of the bistatic scattering echoes to the crop parameters. The simulated results for soybean show that the bistatic specular scattering echoes are more sensitive to crop height and leaf size in C band because vegetation scattering is dominant at high frequency. The wheat scattering coefficients for $\theta_s = \theta_i$ in the forward plane ($\varphi_i = 0^\circ$) and in the plane perpendicular to the incident wave ($\varphi_i = 180^\circ$) are also sensitive to the vegetation moisture in C band. Meanwhile, the specular scattering echoes for wheat in L band are more sensitive to the down layer soil moisture because soil surface scattering is dominant in the specular scattering direction at low frequency. This result is particularly obvious for VV polarization, which is consistent with the backscattering configuration [31, 34]. However, the sensitivity of bistatic scattering coefficients to the vegetation parameters is further determined to be superior to the backscattering configuration.

(3) The maximum of bistatic scattering echoes from wheat and soybean always occurs in the specular scattering direction. However, the minimum of the specular scattering echoes exists in the scattering planes $\varphi_s = 90^\circ$ and $\varphi_s < 90^\circ$ for the HH and VV polarizations, respectively, which is similar to that for soil surface [5]. The minimum location of scattering echoes in VV polarization is determined by the incident wave and the vegetation parameters, which may help retrieve the vegetation parameters in the future. Meanwhile, this minimum characteristic has the potential to detect the targets when the scattering coefficients from vegetations are small and those from targets are highlighted. Therefore, the locations near the minimum scattering echoes are significant for military and civilian applications.

Thoroughly, the investigation of the bistatic scattering characteristics for vegetations is important in providing reference for crop monitoring, environment change prediction, target detection and future bistatic system design. Further studies on conducting bistatic measurement and validating the bistatic scattering models comprehensively are in progress.

ACKNOWLEDGMENT

This paper is supported by Fundamental Research Funds for the Central Universities and National Natural Science Foundation of China (Grant No. 61571355).

REFERENCES

1. Dabrowska-Zielinska, K., et al., "Inferring the effect of plant and soil variables on C-and L-band SAR backscatter over agricultural fields, based on model analysis," *Advances in Space Research*, Vol. 39, 139–148, 2007.
2. Liao, J., T. Xu, and G. Shen, "Simulating microwave scattering for wetland vegetation in poyang lake, southeast china, using a coherent scattering model," *Remote Sensing*, Vol. 7, No. 8, 9796–9821, 2015.
3. Yang, L. and L. Hao, "Numerical modeling and mechanism analysis of vhf wave propagation in forested environments using the equivalent slab model," *Progress In Electromagnetics Research*, Vol. 91, 17–34, 2009.
4. Garcia-Rubia, J. M., O. Kilic, V. Dang, Q. Nguyen, and N. Tran, "Analysis of moving human micro-doppler signature in forest environments," *Progress In Electromagnetics Research*, Vol. 148, 1-14,2014.
5. Johnson, J. T. and J. D. Ouellette, "Polarization features in bistatic scattering from rough surfaces," *IEEE Transactions on Geoscience and Remote Sensing*, Vol. 52, No. 3, 1616–1626, 2014.
6. Nashashibi, A. Y. and F. T. Ulaby, "MMW polarimetric radar bistatic scattering from a random surface," *IEEE Transactions on Geoscience and Remote Sensing*, Vol. 45, No. 6, 1743–1755, 2007.
7. Schlund, M., F. V. Poncet, D. H. Hoekman, S. Kuntz, and C. Schmullius, "Importance of bistatic SAR Features from TanDEM-X for forest mapping and monitoring," *Remote Sensing of Environment*, Vol. 151, No. 8, 16–26, 2014.
8. Gupta, D. K., P. Kumar, V. N. Mishra, R. Prasad, P. K. S. Dikshit, S. B. Dwivedi, A. Ohri, R. S. Singh, and V. Srivastava, "Bistatic measurements for the estimation of Rice crop variables using artifical neural network," *Advances in Space Reasearch*, Vol. 55, 1613–1623, 2015.
9. Bellez, S., H. Roussel, C. Dahon, and J. M. Geffrin, "A rigorous forest scattering model validation through comparison with indoor bistatic scattering measurements," *Progress In Electromagnetics Research B*, Vol. 33, 1–19, 2011.
10. Thirion-Lefevre, L., E. Colin-Koeniguer, and C. Dahon,"Bistatic scattering from forest components. Part I: coherent polarimetric modelling and analysis of simulated results," *Waves in Random and Complex Media*, Vol. 20, No. 1, 36–61, 2010.
11. Ulaby, F. T., K. Sarabandi, K. Mcdonald, M. Whitt, and M. C. Dobson, "Michigan microwave canopy scattering model," *International Journal of Remote Sensing*, Vol. 11, No. 7, 1223–1253, 1990.
12. Toure, A., K. P. B. Thomson, G. Edwards, R. J. Brown, and B. G. Btisco, "Adaptation of the MIMICS backscattering model to the agricultural context-wheat and canola at L and C bands," *IEEE Transactions on Geoscience & Remote Sensing*, Vol. 32, No. 1, 47–61, 1994.
13. Mattia, F., T. L. Toan, G. Picard, F. I. Posa, A. D'Alessio, C. Notarnicola, A. M. Gatti, M. Rinaldi, G. Satalino, and G. Pasquariello, "Multitemporal C-band radar measurements on wheat fields," *IEEE Transactions on Geoscience & Remote Sensing*, Vol. 41, No. 7, 1551–1560, 2003.
14. Huang, B., Y. Chen, L. He, L. Tong, and Y. Wang, "Backscattering modeling of wheat using vector radiative transfer theory," *Journal of Applied Remote Sensing*, Vol. 9, 2015.
15. Kweon, S. K., J. H. Hwang, and Y. S. Oh, "Development of a scattering model for soybean fields and verification with scatterometer and SAR data at X-band," *Journal of Electromagnetic Engineering and Science*, Vol. 12, No. 1, 115–121, 2012.
16. Du, Y., Y. L. Luo, and W. Z. Yan, "An electromagnetic scattering model for soybean canopy," *Progress In Electromagnetics Research*, Vol. 79, 209–223, 2008.

17. Champion, I., L. Préot, and G. Guyot, "Generalized semi-empirical modelling of wheat radar response," *International Journal of Remote Sensing*, Vol. 21, No. 9, 1945–1951, 2000.
18. De Roo, R. D., Y. Du, F. T. Ulaby, and M. C. Dobson, "A semi-empirical backscattering model at L-band and C-band for a soybean canopy with soil moisture inversion," *IEEE Transactions on Geoscience & Remote Sensing*, Vol. 39, No. 4, 864–872, 2001.
19. Kweon, S. K. and Y. Oh, "A modified water-cloud model with leaf angle parameters for microwave backscattering from agricultural field," *IEEE Transactions on Geoscience and Remote Sensing*, Vol. 53, No. 5, 2802–2809, 2015.
20. Kim, Y., T. Jackson, R. Bindlish, H. Lee, and S. Hong, "Monitoring soybean growth using L-, C-, and X-band scatterometer data," *International Journal of Remote Sensing*, Vol. 34, No. 11, 4069–4082, 2013.
21. Jia, M., L. Tong, Y. Zhang, and Y. Chen, "Multitemporal radar backscattering measurement of wheat fields using multifrequency (L, S, C, and X) and full-polarization," *Radio Science*, Vol. 48, 471–481, 2013.
22. Prakash, R., D. Singh, and N. P. Pathak, "The effect of soil texture in soil moisture retrieval for specular scattering at c-band," *Progress In Electromagnetics Research*, Vol. 108, No. 4, 177–204, 2010.
23. Brogioni, M., S. Pettinato, G. Macelloni, S. Paloscia, P. Pampaloni, N. Pierdicca, and F. Ticconi, "Sensitivity of bistatic scattering to soil moisture and surface roughness of bare soils," *International Journal of Remote Sensing*, Vol. 31, No. 15, 4227–4255, 2010.
24. Mittal, G. and D. Singh, "Critical analysis of microwave specular scattering response on roughness parameter and moisture content for bare periodic rough surfaces and its retrieva," *Progress In Electromagnetics Research*, Vol. 100, 129–152, 2010.
25. Mclaughlin, D. J., Y. Wu, W. G. Stevens, X. Zhang, M. J. Sowa, and B. Weijers, "Fully polarimetric bistatic radar scattering behavior of forested hills," *IEEE Transactions on Antennas and Propagation*, Vol. 50, No. 2, 101–110, 2002.
26. Liang, P., M. Moghaddam, L. E. Pierce, and R. M. Lucas, "Radar backscattering model for multilayer mixed-species forests," *IEEE Transactions on Geoscience and Remote Sensing*, Vol. 43, No. 11, 2612–2626, 2005.
27. Ferrazzoli, P., L. Guerriero, and D. Solimini, "Simulating bistatic scatter from surfaces covered with vegetation," *Journal of Electromagnetic Waves and Applications*, Vol. 14, No. 2, 233–248, 2000.
28. Karam, M. A., A. K. Fung, and Y. M. M. Antar, "Electromagnetic wave scattering from some vegetation samples," *IEEE Transactions on Geoscience and Remote Sensing*, Vol. 26, No. 6, 1988.
29. Ulaby, F. T. and M. A. Elrayes, "Microwave dielectric spectrum of vegetation — part II: Dual-dispersion model," *IEEE Transactions on Geoscience and Remote Sensing*, Vol. 25, No. 5, 550–557, 1987.
30. Vine, D. M. L. and M. A. Karam, "Dependence of attenuation in a vegetation canopy on frequency and plant water content," *IEEE Transactions on Geoscience and Remote Sensing*, Vol. 34, No. 5, 1090–1096, 1996.
31. Tiwari, R., R. K. Singh, D. S. Chauhan, O. P. Singh, R. Prakash, and D. Singh, "Microwave scattering for soil texture at X-band and its retrieval using genetic algorithm," *Advances in Remote Sensing*, Vol. 3, 120–127, 2014.
32. Pierdicca, N., L. Pulvirenti, F. Ticconi, and M. Brogioni, "Radar bistatic configurations for soil moisture retrieval: A simulation study," *IEEE Transactions on Geoscience and Remote Sensing*, Vol. 46, No. 10, 3252–3264, 2008.
33. Prakash, R., D. Singh, and N. P. Pathak, "Microwave specular scattering response of soil texture at X-band," *Advances in Space Research*, Vol. 44, No. 7, 801–814, 2009.
34. Bindlish, R. and A. P. Barros,"Parameterization of vegetation backscatter in radar-based, soil moisture estimation," *Remote Sensing of Environment*, Vol. 76, No. 1, 130–137, 2001.